ELSEVIER

Contents lists available at ScienceDirect

Coastal Engineering

journal homepage: www.elsevier.com/locate/coastaleng





Improvement of empirical formulas to estimate the reduction effects by berms on irregular wave runup over a dune-berm coast

Masatoshi Yuhi ^{a,*}, Hajime Mase ^{b,c,d,e}, Daniel T. Cox ^f, Hyoungsu Park ^g

- ^a School of Geosciences and Civil Engineering, Kanazawa University, Kakuma-machi, Kanazawa, 920-1192, Japan
- ^b Disaster Prevention Research Institute, Kyoto University, Gokasho, Uji, Kyoto, 611-0011, Japan
- ^c Toa Corporation, Anzen Cho 1-3, Kanagawa, 230-0035, Japan
- ^d Nikken Kogaku Co., Ltd., Nishishinjuku Bld. 17F, Nishishinnjuku, Tokyo, 160-0023, Japan
- e Hydro Technology Inst., Co., Ltd., Nakanoshima Daibiru 26F, Osaka, 530-6126, Japan
- f School of Civil and Construction Engineering, Oregon State University, Corvallis, OR, 97331, USA
- g Department of Civil and Environmental Engineering, University of Hawaii at Mānoa, Honolulu, HI, 96822, USA

ARTICLE INFO

Keywords: Wave runup Reduction factor Berm Dune Conversion formula Empirical model

ABSTRACT

This study formulates the reduction effects of a sandy berm on irregular wave runup over a dune-berm coast. The numerical experiments by Park and Cox (2016) are closely re-examined to develop an empirical formula describing the variability of reduction effects of a sandy berm over a broad range of conditions. Based on a sequence of regression analyses, the reduction effects are expressed as a reduction factor in terms of normalized berm width, normalized surge level, and wave steepness in deep water. The comparison with the numerical experiments demonstrates that the regression formula can satisfactorily reproduce the variability of the reduction effects over the range of numerical experiments. The analysis of prediction uncertainty demonstrated that the derived formula reproduced the reduction effects observed in the numerical experiments with negligible bias and a 90% confidence interval of approximately $\pm 20\%$ relative error. In addition, conversion formulas between representative runup values based on different statistical definitions are derived to enable consistent comparisons between them. The proposed reduction formula is implemented into three empirical runup models that are applicable to the quick estimations of irregular wave runup on a dune-berm coast: the models by Park and Cox (2016), Stockdon et al. (2006), and Mase et al. (2013). Consistent comparisons were conducted among the empirical predictions and numerical experiments based on the statistical conversion formulas. Combined with the proposed reduction formula, all three models well reproduced the normalized 2% runup in the numerical experiments over a wide range of conditions. On the other hand, the uncertainty in the runup prediction appeared in different forms depending on the selected model. When the proposed reduction formula was implemented in the modified Park and Cox (2016) and modified Stockdon et al. (2006) models, the uncertainty was described by a log-normal distribution of the error ratio between the empirical predictions and numerical experiments. Quantitatively, these two models predicted 90% of the normalized runup on a dune within a range of relative error of less than approximately 20-30%. When the proposed reduction formula was combined with the model by Mase et al. (2013), the uncertainty followed a normal distribution of the residual error between the empirical predictions and numerical experiments. On the normalized runup, the model prediction indicated a small conservative bias (+0.05) and a root-mean-square error of 0.13.

1. Introduction

The concentration of economic activities and efficient land use in the coastal area continues to increase in the 21 century worldwide. At the same time, expected future climate change may impact the coastal area

through extreme wave runup and overtopping exacerbated by sea-level rise and intensified typhoons/cyclones/hurricanes (e.g., Almar et al., 2021; Vitousek et al., 2017). The systematic management of coastal hazard-mitigation infrastructure is necessary to reduce the vulnerability of the coastal assets (e.g., Burcharth et al., 2014; Sekimoto et al., 2013)

E-mail address: yuhi@se.kanazawa-u.ac.jp (M. Yuhi).

^{*} Corresponding author.

against the predicted maximum storm surges and violent waves in the future. Further developments of sophisticated mitigation measures are crucial for coastal disaster prevention, and the adaptation scheme can be improved by realistic and efficient predictions of wave runup and overtopping.

Many studies have enhanced our physical understanding of the nature of wave runup and overtopping on beaches as well as on coastal structures in the past. Based on the research achievements during the past decades, the EurOtop manual (EurOtop, 2007, 2018) and other literature (e.g., U.S. Army Corps of Engineers, 2002; Technical Advisory Committee on Flood Defense (TAW), 2002; Coastal Development Institute of Technology, 2018) have provided state-of-the-art design procedures for coastal defense facilities against the impact of extreme waves. Among the various aspects related to wave runup and overtopping, this study focuses on developing an accurate and efficient prediction method for the runup of irregular waves over a dune-berm coast.

The previous studies revealed that basic characteristics of runup are closely related to the Iribarren number, also called the surf-similarity parameter (Battjes, 1974). Various prediction models have been proposed by investigating the relation between runup and the Iribarren number. Mase et al. (2013) and Park and Cox (2016) reviewed the developments of empirical runup prediction models. When the beach has relatively simple bathymetry, the application of the empirical runup models is straightforward. However, additional factors can influence the runup property when the beach has a compound profile. Specifically, this study treats the influence of a berm in front of a natural dune (or a coastal structure built on the land) on irregular wave runup.

In general, a wide berm can substantially reduce the wave runup over the dunes or structures behind it (e.g., EurOtop, 2007, 2018). Existing studies revealed that the width of a berm and the relative surge/tide level (water depth above the berm) primarily control the reduction of runup level. Recently, Park and Cox (2016) (hereafter referred to as PC2016) conducted systematic numerical experiments for an idealized dune-berm-foreshore system and investigated the dissipative effects of the berm. They proposed a method to account for the reduction effects of wide berms on the runup level on the dune. TAW (2002) and EurOtop (2007, 2018) also proposed prediction formulas for the runup reduction effects of berms.

Nevertheless, our prediction capability of the runup reduction by wide berms is still incomplete. Further efforts are needed to improve the prediction method for a wide range of installation conditions of coastal facilities as well as configurations of dune-berm-foreshore systems. For example, PC2016 utilized different beach slopes to formulate the Iribarren number in the runup estimation. The selective use of the slope is based on the relative surge level. However, the application of this method is not straightforward to other runup models based on equivalent slope concepts (e.g., Saville, 1958; Nakamura et al., 1972; Mase et al., 2013). Moreover, some of the existing prediction models use wave properties in deep water, while others are based on properties at the toe of the structure. The method prescribed in EurOtop and TAW is applicable only for the latter type, which is difficult to be applied to the structures built on the land. Furthermore, in data processing, some studies define the statistical properties of wave runup based on the number of incident waves in deep water, while others utilize the number of runup waves. Therefore, a conversion method is necessary to treat the runup values based on such different definitions consistently. The present study aims at resolving these problems.

More specifically, this study reformulates the reduction factor of irregular wave runup proposed in PC2016 for a dune-berm coast. In the revised formulation, the influence of the relative berm width to the incident wavelength and relative surge elevation to the berm level are described more precisely. In addition, the effect of the offshore wave steepness is incorporated. The reduction factor is expressed as an explicit function of these three dimensionless parameters that can be directly implemented into empirical runup prediction models. The

reproducibility of the reduction effects is examined over a wide range of conditions. The conversion rate among the runups based on different statistical definitions is also studied. The proposed reduction formula is then implemented into three kinds of empirical runup models that are applicable to the quick estimations of irregular wave runup on a dune-berm coast: The models proposed in PC2016 and in Stockdon et al. (2006) are reformulated with the new reduction factor to improve their applicability. Furthermore, the revised formulation is implemented into a model that was developed independently with PC2016 based on the equivalent slope concept: the model by Mase et al. (2013) (IFORM: Integrated Formula of Overtopping and Runup modeling). The applicability of the combined use of these models and the proposed reduction formula are verified through comparison with numerical experiments.

This paper is organized as follows: Section 2 describes the datasets and methods used in this study. The model development and examination are shown in Section 3. First, the general characteristics of the numerical experiments in PC2016 are re-examined in Section 3.1. Next, the variability of the reduction effects is inspected in detail to clarify the characteristics of the influences of berm width, surge level, and wave steepness in deep water. The dissipative effects of berms are then formulated in a compact form as a reduction factor in terms of three dimensionless parameters. The performance of the resulting expression is examined against the numerical experiments in Section 3.2. In addition, a conversion formula is developed and validated to conduct a consistent comparison between the runup based on different statistical definitions in Section 3.3. The proposed formulas of reduction effects and statistical conversion are then implemented into existing runup prediction models. The prediction capability of the proposed method is evaluated by the comparison with the numerical experiments in Section 3.4. The limitation of the proposed model and possibilities for further applications are discussed in Section 3.5. Finally, the main outcomes are summarized in Section 4. The symbols used in the paper are defined when first used.

2. Methodology

2.1. Extracted datasets from the numerical experiments by Park and Cox (2016)

PC2016 conducted systematic numerical experiments to investigate the influence of the berm width and the relative surge level on the runup characteristics of irregular waves over a dune-berm-foreshore system. The runup variability was examined against the representative ranges of berm width and the surge level induced by storm tides. The conditions for the external forces related to waves and tides were determined by referring to the field observations for four hurricanes that had impacted the shoreline in the United States. Fig. 1 describes the geometry of the cross-sectional shape of the bed in the numerical experiments. An idealized dune-berm-foreshore system is characterized by a berm height (h_B) with respect to the still water line, berm width (W_B) , dune height (h_D) with respect to the berm level, and dune width on the berm level (W_D) . The berm profile was set to be horizontal. By referring to the observed field data in the literature, the dune profile was modeled as an idealized Gaussian shape. The use of the Gaussian shape enabled a smooth connection to the flat berm at the merging point, which is necessary to avoid unrealistic reflections in the numerical experiments. The standard deviation of the dune shape was chosen to match the field observations for a realistic dune (Fig. 1). The foreshore was approximated based on the extended equilibrium profile proposed by Romańczyk et al. (2005). In the offshore area of x > 1600 m, the water depth was set constant as 20 m. The representative geometry of the berms and dunes was determined by referring to the field observation at five beaches in the United States. More detailed information can be found in PC2016.

During extreme storm events, few field observations on runup are available (e.g., Senechal et al., 2011). Moreover, the field observations

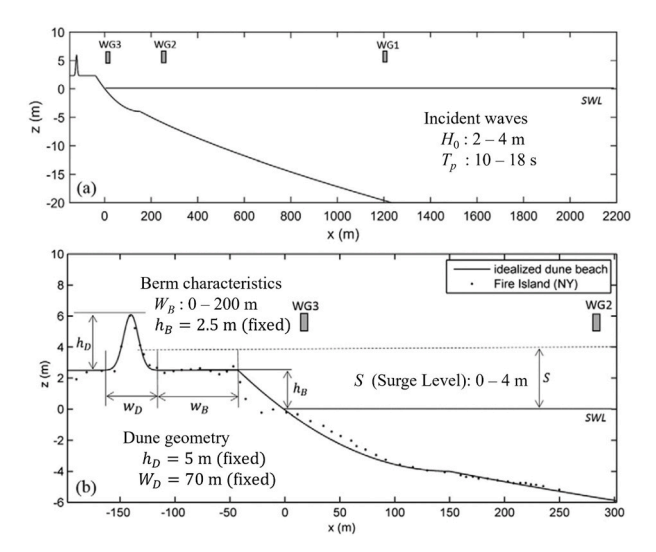


Fig. 1. Overview of the numerical experiments by Park and Cox (2016) (reproduced from Park and Cox (2016)). (a) Modeled cross-shore profile, and (b) detailed view of the dune-berm-foreshore system. The dotted line shows the field profile at Fire Island, NY, by Kraus and Rosati (1997). The dune profile was modeled as $z = h_D \exp(-0.5(x - x_{dc})^2/\sigma^2)$ in which x_{dc} is the location of the dune crest. Based on the literature review on the field observation, the following set was used to model the realistic dune shape: $h_D = 5$ m, $W_D = 70$ m, $\sigma = 10$ m.

of wave run-up during extreme wave conditions over a dune-berm coast are extremely scarce. The use of a state-of-the-art numerical model is considered to be an effective alternative. Accordingly, a non-linear and dispersive wave model, COULWAVE (Lynett et al., 2002), was used to provide synthetic data set of numerical experiments for the evaluation of the dissipation effects of berms. This model is based on the extended Boussinesq equations and high-order finite volume scheme. It has been widely applied to simulate the wave runup and overtopping induced by tsunamis or violent waves due to hurricanes. The applicability has been validated against various hydraulic experiments and field observations (e.g., Lynett and Liu, 2005; Lynett et al., 2002; Lynett et al., 2003; Lynett et al., 2010; Park et al., 2013). Prior to the numerical experiments with wide berms, a series of computations were carried out in PC2016 for the cases without berms to perform the validation of wave generation and the adjustments of several parameters in the numerical model.

Existing studies (e.g., Guza and Thornton, 1982; among others) have indicated that low-frequency motions evolve as incident waves propagate over the surf/swash zones and play an essential role in the wave runup (Raubenheimer and Guza, 1996; Ruggiero et al., 2001). Low-frequency motions are generated by non-linear interaction of waves and uprush-downrush interaction, which result in the reduction of the number of runup waves (Mase, 1995); the resulting reduction of runups

can be captured by the Boussinesq model. In PC2016, the capability of the time-dependent numerical model was examined against the low-frequency motions. The transition of the spectral energy density in the numerical test revealed that the numerical model could adequately reproduce the low-frequency motions relevant to wave runup. However, we should here note that low-frequency waves generally propagate along the coastline in a three-dimensional pattern. Such three-dimensional characteristics cannot be captured in the vertically-two-dimensional computational model used in this study.

Among the numerical experiments by Park and Cox (2016), the results for Cases 3A - 3E were examined in the present study. The corresponding conditions were significant wave height in the deep water of $2.0 \leq H_0 \leq 4.0$ m, peak period of $10 \leq T_p \leq 18$ s, surge level of $1.0 \leq S \leq 4.0$ m, and berm width of $0 \leq W_B \leq 200$ m (Table 1). The berm height, the dune height, and the dune width were fixed as $h_B{=}2.5$ m, $h_D{=}5.0$ m, and $W_D{=}70$ m, respectively. Approximately 250 waves were generated for each run in the numerical experiments.

First, the numerical results were rearranged into a series of subsets. In each subset, the experimental conditions were the same except for the berm width. Every subset included a case with no berm (W_B =0 m) and four cases with a berm of finite width (W_B =25, 55, 100, 200 m). Only the conditions where the runup exceeded the berm height were analyzed in this study. In total, 70 subsets consisting of 350 cases were extracted.

In general, $R_{2\%}$, which is defined as the runup exceeded by 2% of waves (Holman, 1986), has been used as the statistical measure in existing studies. On the other hand, the average of the highest 2% runup events was used as a representative runup in PC2016. In this paper, this quantity is denoted as $R_{1/50}$ for clarity. Under the assumption of Rayleigh distribution, these two quantities are related to each other by

$$R_{1/50} = 1.12R_{2\%} \tag{1}$$

This relation is assumed in the rest of the paper, and $R_{2\%}$ is used as the representative statistical measure of the runup in this study unless otherwise mentioned.

2.2. Modeling of runup reduction effects by a berm

The present study focused on the relationship among the normalized 2% runup $(R_{2\%}^*)$, normalized berm width (W_B^*) , normalized relative surge level (S^*) , and the wave slope in deep water (G^*) . These dimensionless parameters were defined as:

$$R_{2\%}^* = \frac{R_{2\%}}{H_0}, \ W_B^* = \frac{W_B}{L_0} \ , \ S^* = \frac{S - h_B}{H_0}, \ G^* = \frac{H_0}{L_0}$$

Hereafter, the relative surge level means the vertical difference between the surge level (S) and the berm surface (h_B). The runup and relative surge level were normalized by the significant deep-water wave height H_0 , and the berm width was normalized with the wavelength in deep water $L_0 = gT_p^2/(2\pi)$ based on the peak period T_p . The ranges of the dimensionless parameters (W_B^* , S^* , G^*) in the numerical experiments

Table 1 Conditions of numerical experiments.

Model Case	No. of Subsets	Berm Width W_B (m)	Surge Level S (m)	Wave Height H_0 (m)	Peak Period T_p (s)	Dimensionless Berm Width W_B^*	Dimensionless Surge Level S*	Wave Steepness <i>G</i> *
3A	70	0	1.0, 1.5, 2.0, 2.5, 3.0, 4.0	2.0, 3.0, 4.0	10, 12, 14, 16, 18	0	-0.54 ~ 0.83	0.004 ~ 0.024
3B	70	25	1.0, 1.5, 2.0, 2.5, 3.0, 4.0	2.0, 3.0, 4.0	10, 12, 14, 16, 18	0.06 ~ 0.16	−0.54 ~ 0.83	0.004 ~ 0.024
3C	70	55	1.0, 1.5, 2.0, 2.5, 3.0, 4.0	2.0, 3.0, 4.0	10, 12, 14, 16, 18	0.13 ~ 0.36	−0.54 ~ 0.83	0.004 ~ 0.024
3D	70	100	1.0, 1.5, 2.0, 2.5, 3.0, 4.0	2.0, 3.0, 4.0	10, 12, 14, 16, 18	0.24 ~ 0.66	−0.54 ~ 0.83	0.004 ~ 0.024
3E	70	200	1.0, 1.5, 2.0, 2.5, 3.0, 4.0	2.0, 3.0, 4.0	10, 12, 14, 16, 18	0.48 ~ 1.31	−0.54 ~ 0.83	0.004 ~ 0.024
Total	350	0 ~ 200	1.0, 1.5, 2.0, 2.5, 3.0, 4.0	2.0, 3.0, 4.0	10, 12, 14, 16, 18	0~1.31	-0.54 ~ 0.83	0.004 ~ 0.024

are summarized in Table 1.

The reduction effects of a berm on a runup on the dune were formulated through the regression to the extracted numerical datasets. First, we compared the runup over a berm (cases of $W_B^* > 0$) to that without the berm (case of $W_B^* = 0$) in the same subset. Note that in each subset, the experimental conditions were the same except for the berm width. The reduction factor of runup on a dune (C) was then defined as the ratio between them.

$$C = \frac{R_{2\%}^{*}(W_{B}^{*} > 0)}{R_{2\%}^{*}(W_{B}^{*} = 0)}$$

We assumed that the variability of C could be expressed as a function of W_B^* , S^* , and G^* . Previous studies demonstrated that W_B^* is a primary parameter describing the variability of C. It is known that C generally decreases with the berm width and approaches asymptotic constants for sufficiently large width (e.g., TAW, 2002; Park and Cox, 2016; EurOtop, 2007, 2018). To describe the correlation between C and W_B^* , PC2016 adopted the hyperbolic tangent function. TAW (2002) and EurOtop (2007, 2018) used a polyline profile, which is qualitatively similar to the hyperbolic tangent profile. Referring to these studies, we have adopted W_B^* as the principal parameter in the regression analysis and assumed the following form:

$$C = 1 - K_1 \tanh(K_2 \cdot W_p^*) \tag{2}$$

The equation above includes two non-dimensional parameters, K_1 and K_2 . PC2016 assumed the same form as Eq. (2), and they assumed that these parameters are constants. In the present study, K_1 and K_2 were determined as a function of S^* and G^* .

The physical meanings of these two parameters are sketched in Fig. 2. The K_1 parameter indicates the maximum reduction effects when W_B^* is sufficiently large, and K_2 is a sensitivity parameter that controls the rate of decrease in C with respect to W_B^* . Large K_2 indicates an intense reduction of R^* with W_B^* and vice versa. The inverse of K_2 is recognized as a measure of the width where the runup reduction tends to saturate.

First, the reduction factors in the numerical experiments were examined.

$$C_{i,j}^{ne} = R_{i,j}^* / R_{i,0}^*$$

In which the subscript i (i=1,2,...,70) indicates the consecutive number assigned for each subset of data. The subscript j indicates the case number within each subset. The conditions of $W_B{}^*=0,25,55,100$, and 200 m corresponds to j=0,1,2,3, and 4, respectively. Hereafter, the superscript 'ne' means the quantities obtained for each run of the numerical experiments.

Then the variability of $C_{i,j}^{ne}$ was approximated as a continuous function of W_B^* in the form of Eq. (2). For each subset, the optimized combination of the two parameters $K_{1,i}^{ss}$ and $K_{2,i}^{ss}$ were determined empirically based on the least square method. Hereafter, the superscript 'ss' means the quantities obtained for each subset.

The resulting variation of $K_{1,i}^{ss}$ was then approximated as a continuous function of S^* and G^* . We assumed that the maximum reduction rate K_1 could be expressed as the product of the two functions K_{11} (S^*) and K_{12}

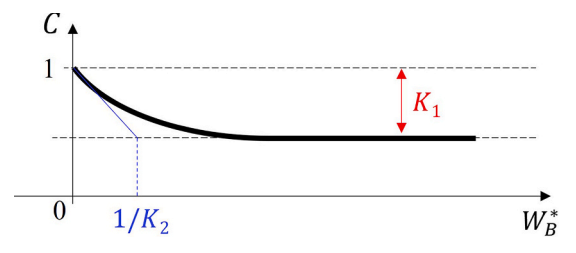


Fig. 2. Schematic expression of the physical meaning of K_1 and K_2 .

 $(G^*).$

$$K_{1:i}^{ss} \cong K_1(S^*, G^*) = K_{11}(S^*)K_{12}(G^*)$$
 (3)

The form of K_{11} and K_{12} were determined through the following two-step procedure. In the first step, we examined the dependence of K_1 on S^* by temporarily assuming $K_{12}=1$. We then formulated K_{11} as a continuous function of S^* . In the second step, we investigated the influence of the wave slope. We examined the relationship between $K_{1,i}^{ss}/K_{11}$ and G^* to express K_{12} as a continuous function of G^* . Next, the reproducibility of the regression formula was confirmed through the comparison between $K_1(S_i^*, G_i^*)$ and $K_{1,i}^{ss}$. Determination and examination of the regression formula for the sensitivity parameter K_2 were conducted similarly.

$$K_{2,i}^{ss} \cong K_2(S^*, G^*) = K_{21}(S^*)K_{22}(G^*)$$

The final regression form of the reduction factor (C) was then described as:

$$C = 1 - K_1 \tanh(K_2 \cdot W_{\rm p}^*) = 1 - K_{11} K_{12} \tanh(K_{21} K_{22} \cdot W_{\rm p}^*)$$
(4)

In the regression analysis, the functional forms of K_{11} , K_{12} , K_{21} , and K_{22} were chosen empirically. The behavior of error between the numerical experiments and empirical formulations was then examined by systematically varying the model coefficients to find out the optimum sets of them that provide the least mean-square error. We have also tried to apply a non-linear fitting method (i.e., the Gauss-Newton method) but found that the non-linear scheme is less robust and that the obtained results indicated insignificant differences.

The performance of the reduction formula was confirmed through the comparison with $C^{ne}_{i,j}$. As a quantitative evaluation, the following analysis was conducted. First, the distribution of the residual error and error ratio between the formula and numerical experiments was investigated: (residual error) $e_{res} = C - C^{ne}_{i,j}$; (error ratio) $e_{ratio} = C/C^{ne}_{i,j}$. The cumulative distributions of e_{res} and $\log(e_{ratio})$ were compared with that of the normal distribution to examine if the distribution of the error follows the normal/log-normal distribution. Based on the resulting type of error distribution, suitable statistical measures were selected and presented. The corresponding 90% confidence interval of the reduction factor C is then provided. The detail of the actual procedure will be explained in Section 3.2.

2.3. Reformulation of the prediction models proposed by Park and Cox (2016)

(i) Overview of PC2016 model

The following prediction model was proposed for $R_{1/50}$ based on the number of runup events in PC2016.

$$\frac{R_{1/50,R}}{H_0} = 1.35C_{PC}\xi_r^{0.65} \tag{5a}$$

where the two constants (1.35 and 0.65) were determined by least-square fitting. The subscript "R" is added in the expression above (and hereafter) to indicate that the corresponding quantity is based on the number of runup events. The ξ_r represents the Iribarren number defined with three kinds of representative beach slopes according to the normalized surge level in PC2016 as follows:

$$\xi_r = \xi_f = \tan \beta_f / \sqrt{H_0/L_0} \quad \text{for } S^* \le -0.7$$
 (5b)

$$\xi_r = \xi_d = \tan \beta_d / \sqrt{H_0/L_0} \quad for S^* \ge 0.7$$
 (5c)

$$\xi_r = \tan \beta_t / \sqrt{H_0/L_0} \quad for \ -0.7 < S^* < 0.7$$
 (5d)

In the equations above, β_f and β_d indicate the foreshore slope and dune slope, respectively. The transition slope β_t varies linearly with S^* :

$$\beta_t = (1 - \alpha)\beta_f + \alpha\beta_D$$
 for $-0.7 < S^* < 0.7$

$$\alpha = 0.5 + S^*/1.4$$

The reduction factor C_{PC} was described as

$$C_{PC} = 0.8 - 0.4 \tanh(2.0W_B^*)$$
 (5e)

$$C_{PC} = 1.0 - 0.5 \tanh(2.0W_p^*)$$
 (5f)

Equation (5e) provided a mean value, while Eq. (5f) provided a conservative estimate. Hereafter this model is referred to as the PC16 model.

(ii) Overview of modified Stockdon model

Based on various field measurements of runup on natural beaches, Stockdon et al. (2006) developed the following runup formula:

$$\frac{R_{2\%,R}}{H_0} = 1.1 \left(0.35\xi_f + 0.5 \left[0.536\xi_f^2 + \frac{0.004}{H_0/L_0} \right]^{0.5} \right)$$

in which ξ_f represents the Iribarren number defined with the foreshore slope. PC2016 demonstrated that if the Iribarren number based on the foreshore slope is used, this model substantially underestimates the runup on the dune in the numerical experiments. They proposed a modification of this model (hereafter mST16 model) in which ξ_r was used instead of ξ_f and C_{PC} was incorporated as a reduction factor related to berm effects:

$$\frac{R_{1/50,R}}{H_0} = 1.1C_{PC} \left(0.35\xi_r + 0.5 \left[0.536\xi_r^2 + \frac{0.004}{H_0/L_0} \right]^{0.5} \right)$$

(iii) Improvements of the formulations in PC16 and mST16 models

The structure of the PC16 and mST16 models reveals that the factor C_{PC} represents the dissipation with the relative width of the berm, while the rest of the formula (e.g., $1.35\xi_r^{0.65}$) represents the runup expected at $W_B^* = 0$. In that sense, the first term of C_{PC} in Eqs. (5e) and (5f) is expected to be equal to 1.0. However, the best fit for the numerical experiments resulted in the value of approximately 0.8 in PC2016 (Eq. (5e)). This implies that the part described by $1.35\xi_r^{0.65}$ overestimates the numerical experiments at $W_B^* = 0$ on the whole. This is probably because the coefficient 1.35 was determined based on ξ_f . It is thus better to reformulate the formula in order to obtain a more consistent form in which the reduction factor is unity at $W_B^* = 0$, and the rest of the formula in terms of ξ_r well reproduces the corresponding runups. For this purpose, we attempt to replace the description of the reduction factor and retune the formula in this study. Also, we should note that although the original Stockdon model was proposed for $R_{2\%,R}$, the mST16 model was applied to the prediction of $R_{1/50,R}$. Besides, in PC2016, PC16 was combined with Eq. (5e), while Eq. (5f) was adopted for mST16 in the performance tests. More unified expression deserves to be pursued. To resolve these points and obtain better formulations, we reformulated these models as follows in this study.

$$\frac{R_{2\%,R}}{H_0} = aC\xi_r^{0.65} \tag{6}$$

$$\frac{R_{2\%,R}}{H_0} = 1.1C \left(0.35\xi_r + 0.5 \left[0.536\xi_r^2 + \frac{0.004}{H_0/L_0} \right]^{0.5} \right)$$
 (7)

where the reduction factor C is expressed by Eq. (4) in a unified form.

The definition of the representative Iribarren number (ξ_r) is the same as in the PC16 and mST16 models (Eqs. (5b) to (5d)). Note that the use of ξ_r is needed to describe the runup on the dune at $W_B^* = 0$ properly in Eqs. (6) and (7). The constant a is adjusted to provide the best fit. The former and latter are referred to as PC22 and mST22 models, respectively.

2.4. Implementation into the runup prediction model by Mase et al. (2013)

Furthermore, the proposed reduction factor was implemented into an empirical prediction model of irregular wave runup, IFORM, that was developed independently with the numerical experiments in PC2016. IFORM is an integrated prediction model for runup and overtopping of irregular waves (Mase et al., 2013, 2016; Tamada et al., 2015; Yuhi et al., 2021). In this model, the normalized 2% runup is estimated by the following formula.

$$\frac{R_{2\%,I}}{H_0} = 2.99 - 2.73 \exp(-0.57\xi_{im})$$
 (8a)

Note that, in IFORM, the 2% runup is defined as the runup exceeded by 2% of incident waves in deep water. The subscript "T" is added hereafter to the runup based on the incident waves $(R_{2\%,I})$. In the equation above, ξ_{im} is the Iribarren number based on the imaginary slope $(\tan\beta_{im})$.

$$\xi_{im} = \frac{\tan \beta_{im}}{\sqrt{H_0/L_0}} \tag{8b}$$

The imaginary slope is defined with the cross-sectional area A between the runup and breaker points (h_{br} : breaker depth) (Fig. 3). It is computed based on the method proposed by Nakamura et al. (1972) through an iterative procedure.

$$\tan \beta_{im} = \frac{\left(h_{br} + R_{2\%,I}\right)^2}{2A} \tag{8c}$$

The definitions of the parameters are graphically shown in Fig. 3. The breaker depth h_{br} over general profiles can be calculated by the numerical model by Mase and Kirby (1993). For planar beach of slope $\tan\beta$, it can be computed by the following equation (Mase et al., 2016).

$$\frac{h_{br}}{H_0} = a_0 + a_1 \exp\left[-\left(\frac{\ln\{(H_0/L_0)/a_2\}}{a_3}\right)^2\right]$$
 (8d)

The coefficients a_0 to a_3 are defined as

$$a_0 = 30.2 - 27.3 \exp\left[-\left\{\frac{\ln(22.9 \tan \beta)}{5.45}\right\}^2\right]$$

$$a_1 = -9.95 + 8.92 \exp\left[-\left\{\frac{\ln(29.4 \tan \beta)}{3.13}\right\}^2\right]$$

$$a_2 = 0.0302 - 0.0023 \exp\left[-\left\{\frac{\ln(25.9 \tan \beta)}{1.71}\right\}^2\right]$$

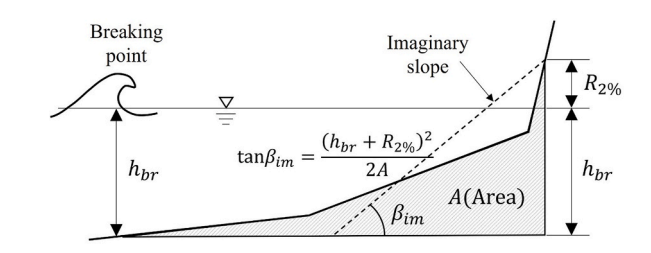


Fig. 3. Definitions of the parameters used in IFORM (according to Nakamura et al., 1972).

$$a_3 = 6.13 - 3.50 \exp \left[-\left\{ \frac{\ln(36.4 \tan \beta)}{1.35} \right\}^2 \right]$$

IFORM is applicable in the range of bed slope >1/100.

The regression formula (4) was implemented into Eq. (8a) in IFORM as a reduction factor representing the dissipative effects of a berm on the runup:

$$\frac{R_{2\%,I}}{H_0} = C(W_B^*, S^*, G^*)[2.99 - 2.73 \exp(-0.57\xi_{im})]$$
 (9)

Here, the computational procedure consisted of three steps. At first, the runup value was computed based on Eq. (8a) for the condition of no berm $(W_B^*=0)$. If the resulting runup exceeded the berm level, the reduction factor C was computed for the given conditions of W_B^* , S^* , and G^* based on Eq. (4). If not, C was set as unity. Finally, the runup for $W_B^*>0$ was computed by multiplying the reduction factor as shown in Eq. (9).

2.5. Conversion formula among the runup based on different definitions

The statistical measures of irregular wave runup used in existing studies are sometimes slightly different. The most widely used quantity is the 2% runup ($R_{2\%}$). The definition of 2% is, however, not necessarily unique. For example, Coastal Engineering Manual (U.S. Army Corps of Engineers, 2002) and EurOtop manual (2018) define the $R_{2\%}$ as the runup level exceeded by the 2% of incident waves $(R_{2\%,I})$. The same definition is adopted in IFORM. In the model of Stockdon et al. (2006), $R_{2\%}$ is based on the runup records ($R_{2\%,R}$). In the numerical experiments by PC2016, as mentioned in Section 2.1, the average of the highest 2% of runup waves $(R_{1/50.R})$ was adopted. For consistent comparison among $R_{2\%,I}$, $R_{2\%,R}$, and $R_{1/50,R}$, the relation between $R_{2\%,I}$ and $R_{2\%,R}$ is needed, since the relation between $R_{1/50,R}$ and $R_{2\%,R}$ is given as Eq. (1). In a precise sense, there remains certain uncertainty in the count of the number of runup events. For example, the zero-cross method and crest method provides different numbers of runup events. However, this aspect is not pursued further in this paper because it is beyond the scope of the present study.

In general, the number of runup events (N_R) is smaller than the number of incident waves at the deep-water boundary (N_I). The reduction in wave number is induced because part of the incoming waves cannot runup over the beach due to the strong back-rush of preceding waves, or some waves running up the beach are overtaken and captured by subsequent waves before reaching maximum runup level (Mase et al., 1983; Mase and Iwagaki, 1985). The reduction in wave number becomes more significant on gently sloping beaches. Because N_R is smaller than N_I , the $R_{2\%}$ with respect to N_R becomes higher than that with respect to N_I . In order to make a consistent comparison between the $R_{2\%}$ computed by different criteria, a conversion formula is needed between them.

In the present study, the ratio between the number of runup waves and incident waves $(n=N_R/N_I)$ was described as a function of the Iribarren number based on the hydraulic experiments by Mase et al. (1983) and Mase and Iwagaki (1985). Furthermore, under the assumption of Rayleigh distribution for the runup (Mase et al., 2004), a conversion formula was established for the $R_{2\%}$ based on different definitions. The detail of the conversion will be explained in Section 3.3.

2.6. Examination of the applicability of the proposed model

Finally, the applicabilities of the proposed reduction formula implemented in PC22, mST22, and IFORM were examined by comparing the predicted dimensionless runup on the dune with those by the numerical experiments. The comparison with the numerical experiments was conducted consistently based on $R_{2\%,R}$. For this purpose, the $R_{1/50,R}$ obtained in the numerical experiments were converted into $R_{2\%,R}$ by Eq. (1), and $R_{2\%,L}$ obtained by IFORM was converted into $R_{2\%,R}$ based on the

proposed conversion formula.

In the numerical simulations, a Gaussian shape was used to express the dune profile. The treatment of the profile was simplified in the empirical prediction models, and the dune shape was characterized by the mean slope: In the prediction by PC22, mST22, and IFORM, the dune slope was fixed at 0.143 ($=h_D/(W_D/2)$). Similarly, the beach slope was set constant as 0.023 in the empirical predictions. This is equivalent to approximating the dune and the foreshore profile by a triangular and a planar shape, respectively, in the course of empirical predictions.

In the performance tests, the residual error (e_{res}) and error ratio (e_{ratio}) between the prediction formula and the numerical experiments were analyzed. The cumulative distribution of e_{res} and $\log(e_{ratio})$ was examined for each model. Depending on the types of the error distributions, we have presented the following statistics: In the cases where e_{res} followed the normal distributions, the root-mean-square error (RMSE), and the bias of the error (Bias) were provided in addition to the coefficient of determination (r^2) . On the other hand, the geometric mean and geometric standard deviation were presented when e_{ratio} followed the log-normal distribution. Based on the obtained information, the 90% confidence interval is estimated.

3. Results and discussion

3.1. General characteristics of reduction effects by a berm on wave runup

First, the general characteristics of the runup reduction induced by a berm were examined in terms of the three non-dimensional parameters. Fig. 4(a) plots the variation of the runup reduction factor $C_{i,j}^{ne}$ against the dimensionless berm width W_B^* in the numerical experiments. Generally, $C_{i,j}^{ne}$ decreases with W_B^* . Besides, the runup reduction effects by a berm have upper limits: When W_B^* is larger than $0.4 \sim 0.6$, $C_{i,j}^{ne}$ asymptotes to constants for given conditions of S^* . These features are consistent with the previous studies. On average, the normalized runup over very wide berms decreases around $40 \sim 70\%$ compared with runups without a berm. Moreover, close inspection reveals that the maximum reduction of runup for large W_B^* and the reduction sensitivity to W_B^* depend on S^* .

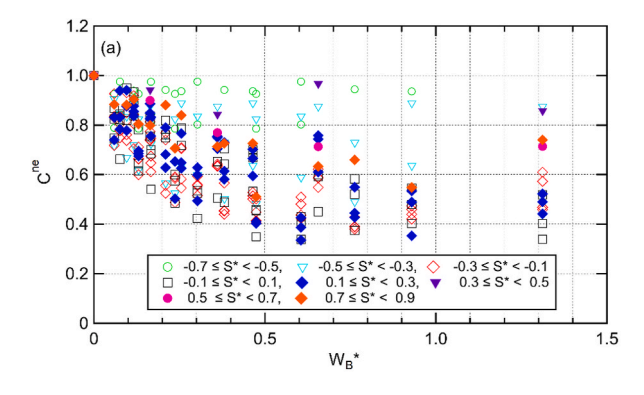
The relation between $C_{i,j}^{ne}$ and S^* is plotted in Fig. 4(b1) and Fig. 4(b2). Although the scatter of plots indicates that the correlation between $C_{i,j}^{ne}$ and S^* is weak compared with W_B^* , the following tendencies are observed. In the area $S^*<0$, $C_{i,j}^{ne}$ decreases with S^* . It takes a minimal peak around $S^*=-0.2\sim0.0$ and then turns to increase with S^* . The observed tendency in the numerical experiments is consistent with the description in EurOtop (2007, 2018) stating that "A berm lying on the still water line is most effective."

The relation between $C_{i,j}^{ne}$ and G^* is plotted in Fig. 4(c). Although the scatter is large and the influence of G^* is weak compared with that of W_B^* and S^* , $C_{i,j}^{ne}$ indicates an increasing tendency with G^* .

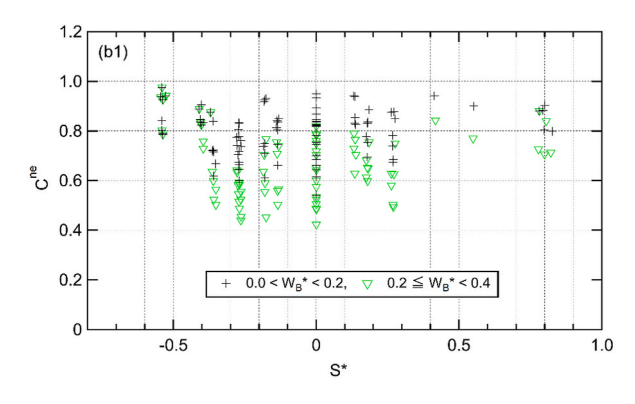
3.2. Modeling of reduction factor

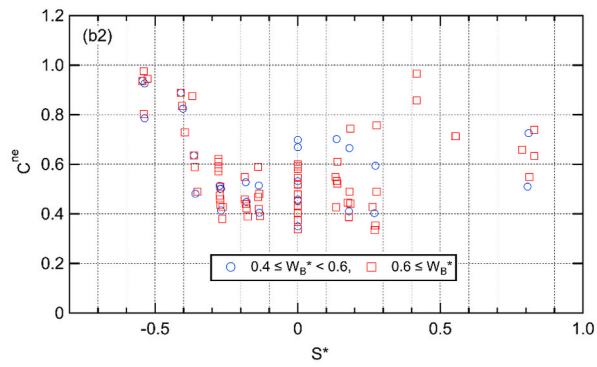
First, the optimum combination of the two parameters K_1 and K_2 in Eq. (2) was obtained empirically for 70 subsets by the least square method. Several examples of the comparison between the numerical experiments ($C_{i,j}^{ne}$) and regressions (C_i^{ss} based on $K_{1,i}^{ss}$ and $K_{2,i}^{ss}$) are shown in Fig. 5.

The maximum reduction rate K_1 was then formulated in the form of Eq. (3). Fig. 6(a) shows the relation between $K_{1,i}^{ss}$ and S^* . As expected from the plots in Fig. 4(b1) and (b2), the reduction becomes most significant around $S^* = 0$. In this plot, the correlation between $K_{1,i}^{ss}$ and S^* shows a substantially different tendency depending on the sign of S^* . Namely, the variability indicates different features depending on whether the surge level is beyond or below the berm level. In the condition where the surge level is below the berm, K_1^{ss} varies with steep gradient in the range $-0.6 < S^* < -0.2$. On the other hand, K_1^{ss} gradually

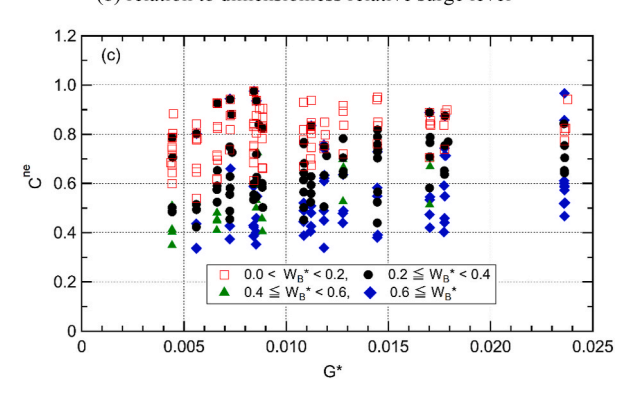


(a) relation to dimensionless berm width





(b) relation to dimensionless relative surge level



(c) relation to wave steepness in deep water

Fig. 4. Relation between runup reduction and non-dimensional parameters. (a) relation to dimensionless berm width, (b) relation to dimensionless relative surge level, (c) relation to wave steepness in deep water. (The cases corresponding to $W_B^*=0$ (C=1) are omitted in (b1), (b2), and (c).)

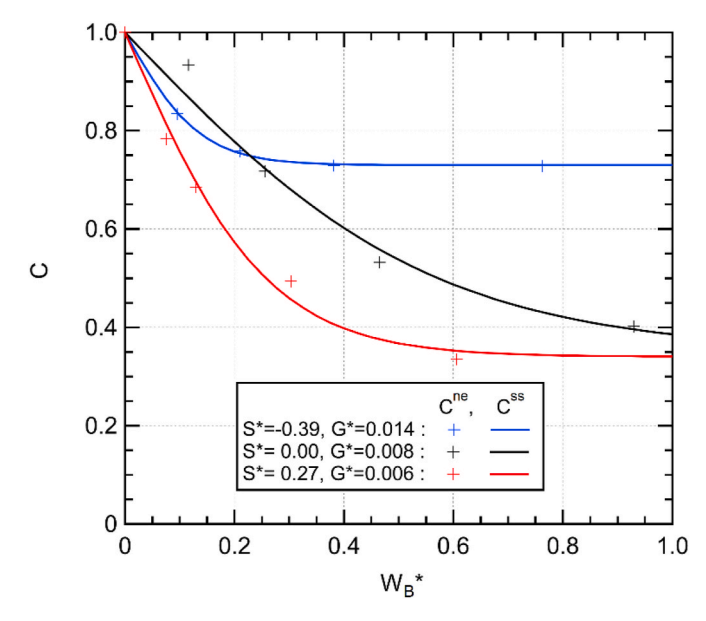
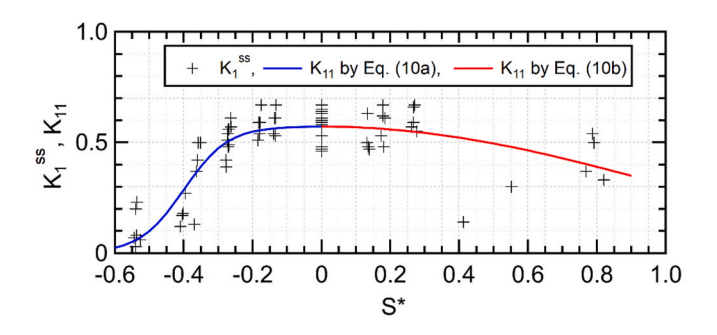
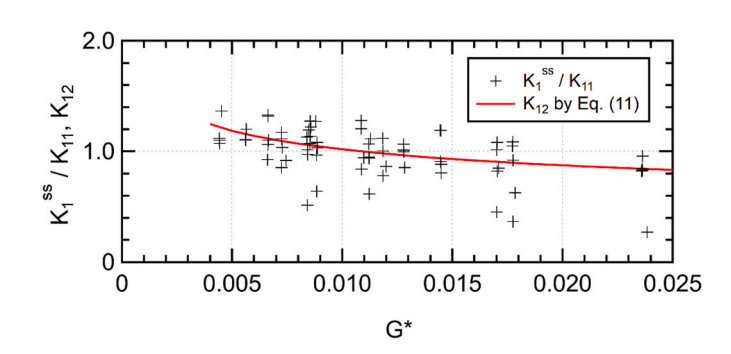


Fig. 5. Examples of the optimized regression for the reduction factor.



(a) relation between K_{11} and S^*



(b) relation between K_{12} and G^*

Fig. 6. Regression analysis for K_1 . (a) relation between K_{11} and S^* , (b) relation between K_{12} and G^* .

decreases in the area $S^*>0$. Based on these observations, the regression curve was divided into two parts. Different forms of function were assigned for each part, and the optimum set of coefficients that provides the least mean-square error was empirically pursued for each function. The regression results were obtained as

$$K_{11} = 0.29[1 + \tanh(7.8(S^* + 0.4))]$$
 for $-0.6 < S^* < 0.0$ (10a)

$$K_{11} = 0.29[1 + \cos(1.5S^*)]$$
 for $0.0 \le S^* < 0.9$ (10b)

In the equations above, the two regression curves were determined to be continuous at the connecting point ($S^*=0$). Regression to K_{11} indicated some scatter in Fig. 6(a). This is partially because the influence of G^* (to be accounted for by the counterpart coefficient K_{12}) is included in $K_1^{\rm ss}$. Besides, the deviation around the regression curves reflects the uncertainty of the model predictions. Similar uncertainty arises in the regression of the other coefficients. This sort of model uncertainty will be discussed later in Section 3.5. Overall, Fig. 6(a) demonstrates that the combined use of the above regression formulas successfully describes the general tendencies of variation observed in the numerical experiments, except for the two points in the range of $0.4 < S^* < 0.6$. We note that TAW (2002) and EurOtop (2007, 2018) also treated the conditions of $S^* < 0$ and $S^* \ge 0$ separately and used the cosine function form for $S^* \ge 0$.

From Fig. 4(c), we can deduce that if the regression formula is established for a medium value of G^* , the reduction rate tends to be underestimated for a small value of G^* , while the reduction is likely to be overestimated for a larger value of G^* . And therefore, the counterpart coefficient K_{12} was introduced as a correction factor. Fig. 6(b) plots the relation between $K_{12}\cong K_{1,i}^{S}/K_{11}$ and G^* . The results indicate that K_{12} decreases gradually with G^* except for two outliers (located beyond the plot range of the figure). After some trials and errors, the relation was approximated as:

$$K_{12} = 0.37(G^*)^{-0.22} \quad (0.004 < G^* < 0.025)$$
 (11)

to provide the least mean square error between K_1 and $K_{1,i}^{ss}$.

The maximum reduction factor was then computed as $K_1 = K_{11}K_{12}$. The results based on regression formulas are compared with K_1^{ss} in Fig. 7. The dotted line represents the perfect match. The qualitative agreement is satisfactory. Quantitatively, the coefficient of determination, RMSE, and bias error is $r^2 = 0.79$, RMSE = 0.08, and Bias = 0.00, respectively. The obtained regression values successfully reproduce the numerical results.

Next, the regression formula for the response sensitivity K_2 was determined. First, the relation between K_{21} and S^* was modeled. Fig. 8 (a) plots the relation between $K_{2,i}^{ss}$ and S^* . In the figure, $K_{2,i}^{ss}$ monotonically decreases with S^* . It changes significantly in the range $-0.6 < S^* < -0.2$. It approaches constant values when $|S^*|$ becomes large on both sides. In order to reproduce these features, the variability of K_{21} was modeled empirically as

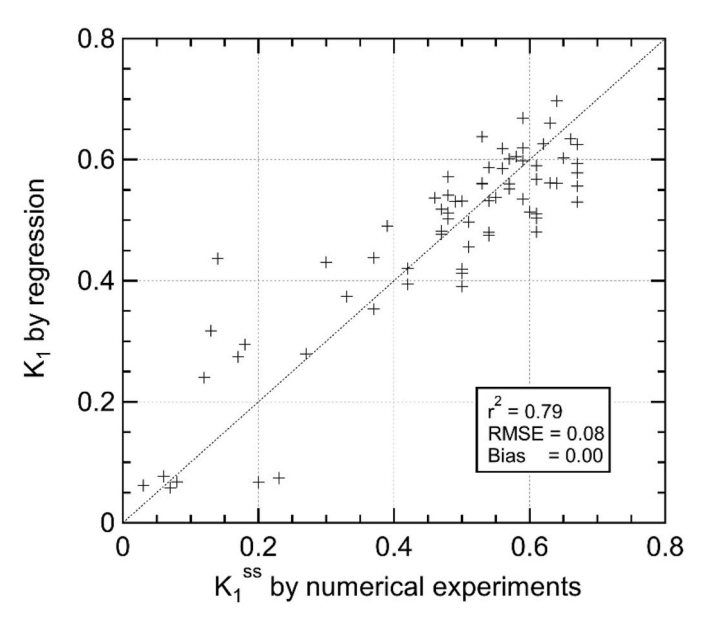
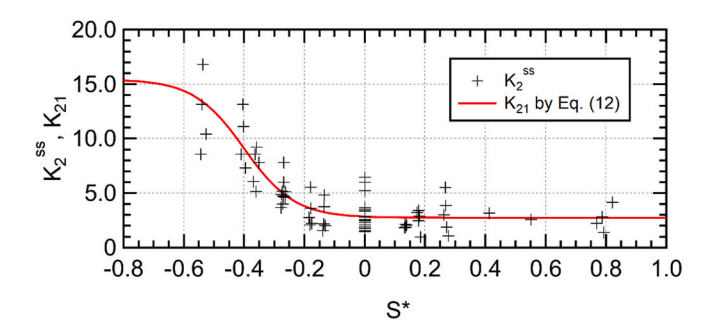
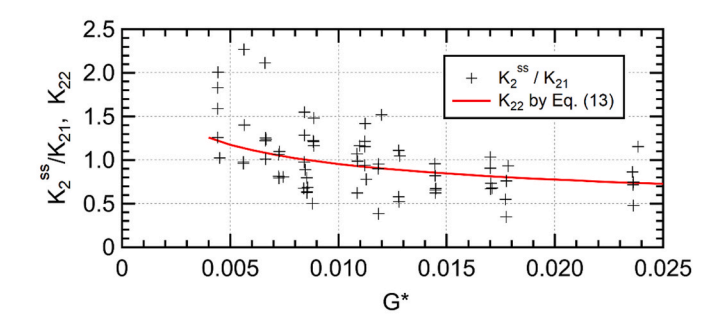


Fig. 7. Comparison between optimum and regression values of K_1 .



(a) relation between K_{21} and S



(b) relation between K_{22} and G^*

Fig. 8. Regression analysis for K_2 . (a) relation between K_{21} and S^* , (b) relation between K_{22} and G^* .

$$K_{21} = -6.4 \tanh(6.0(S^* + 0.4)) + 9.1 \quad (-0.6 < S^* < 0.9)$$
 (12)

Next, the counterpart coefficient K_{22} was introduced as a correction factor. Fig. 8(b) plots the relation between $K_{22} \cong K_{2,i}^{\text{S}}/K_{21}$ and G^* . The results indicate that K_{22} decreases gradually with G^* except for several outliers. Thus, the relation was formulated as:

$$K_{22} = 0.24 (G^*)^{-0.30} \quad (0.004 < G^* < 0.025)$$
 (13)

to provide the least mean square error between K_2 and K_2^{ss} .

The K_2 parameter was then computed as $K_2 = K_{21}K_{22}$. The results are

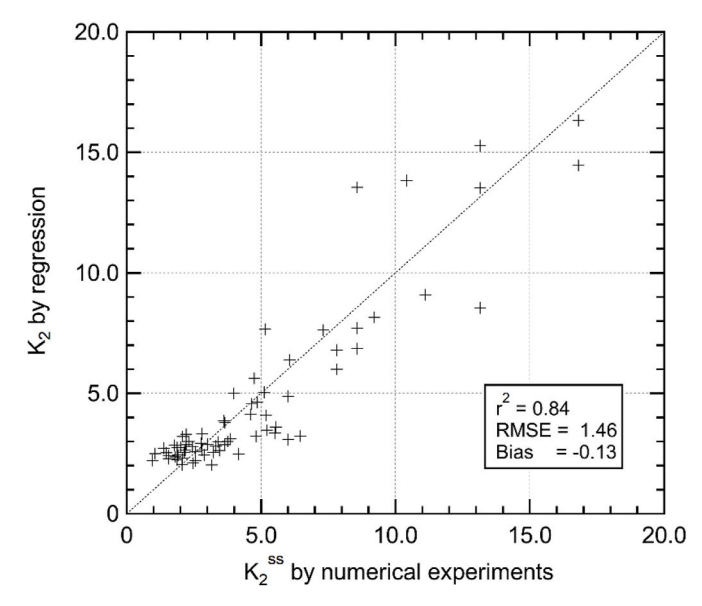
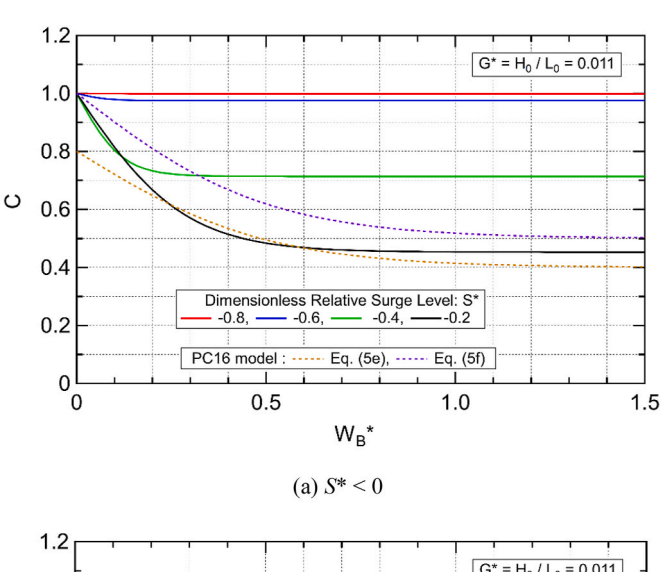


Fig. 9. Comparison between optimum and regression values of K_2 .

compared with $K_2^{\rm ss}$ in Fig. 9. The dotted line represents the perfect match. The coefficient of determination, RMSE, and bias error are $r^2=0.84$, RMSE = 1.46, and Bias = -0.13, respectively.

The reduction factor expressed by Eq. (4) is plotted against the normalized berm width in Fig. 10 for different values of S^* . In this figure, the deep-water wave slope is fixed as $G^*=0.011$ (the mean value of the numerical experiments). We can recognize the characteristics of the variation of the reduction curve with respect to S^* from these figures. The reduction becomes most significant in the range $-0.2 < S^* < 0.0$. Under this condition, the runup could be reduced to less than half without a berm. The reduction rapidly asymptotes to a constant when the surface level is far below the berm ($S^* < -0.4$).

As additional tests of the performance of the regression formula, Fig. 11 compare the variation of the reduction factor C against W_B^* in the numerical experiments and regression curves. The comparisons are carried out for five ranges of S^* . Two examples are shown in Fig. 11. The marker plots in the figures represent the numerical experiments, and the solid lines indicate the regression results. The red line corresponds to the middle range of the conditions for S^* and G^* in each figure. The green and blue lines roughly correspond to the estimated upper and lower limit of the predicted values in the range of each situation, respectively. The scatter in each figure mostly lies between the green and blue lines. The reproducibility in other ranges is satisfactory as well as in Fig. 11. These results demonstrate the high applicability of the proposed formula to express the variability of runup reduction induced by a berm.



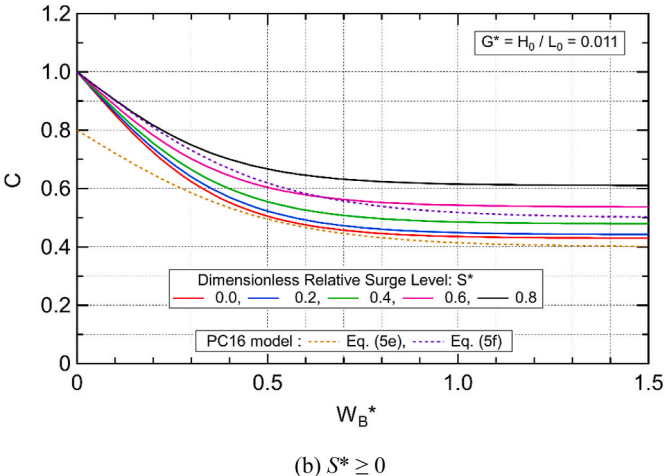
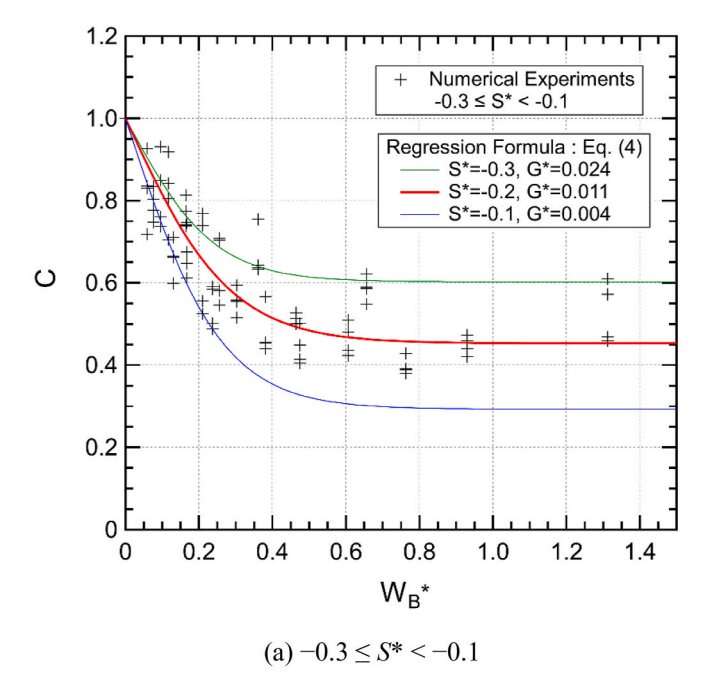


Fig. 10. Model relation among the runup reduction factor and dimensionless berm width and dimensionless relative surge level ($G^*=H_0/L_0=0.011$). (a) $S^*<0$, (b) $S^*\geq0$.



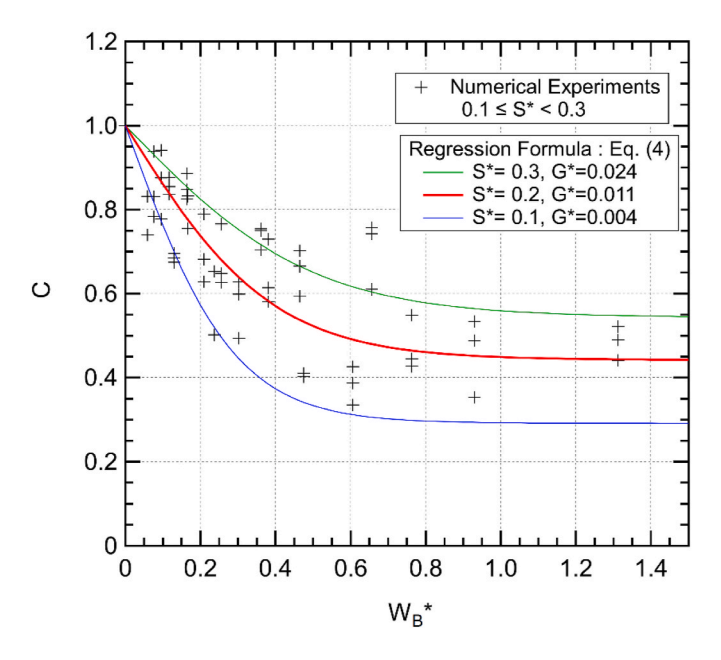


Fig. 11. Comparison of the predicted runup reduction and numerical experiments. (a) $-0.3 \le S^* < -0.1$, (b) $0.1 \le S^* < 0.3$.

(b) $0.1 \le S^* < 0.3$

Finally, we compared the computed reduction factors with the numerical experiments in Fig. 12. The results indicate that the regression formula can reproduce the variability of $C_{i,j}^{ne}$ over the range of numerical experiments very well with the high correlation of $r^2=0.88$. The analysis of error distribution reveals that e_{ratio} closely follows the lognormal distribution. The geometric mean was 1.00: Namely, the prediction formula indicates a negligible bias. In other words, the reduction formula provides the 50% exceedance level of the numerical experiments (the blue line in Fig. 12). The corresponding geometric standard deviation was 1.12. Under the assumption of log-normal distribution for e_{ratio} , 90% of plots are located within the relative error range of approximately 20%. This interval is indicated by purple lines in Fig. 12.

M. Yuhi et al. Coastal Engineering 176 (2022) 104166

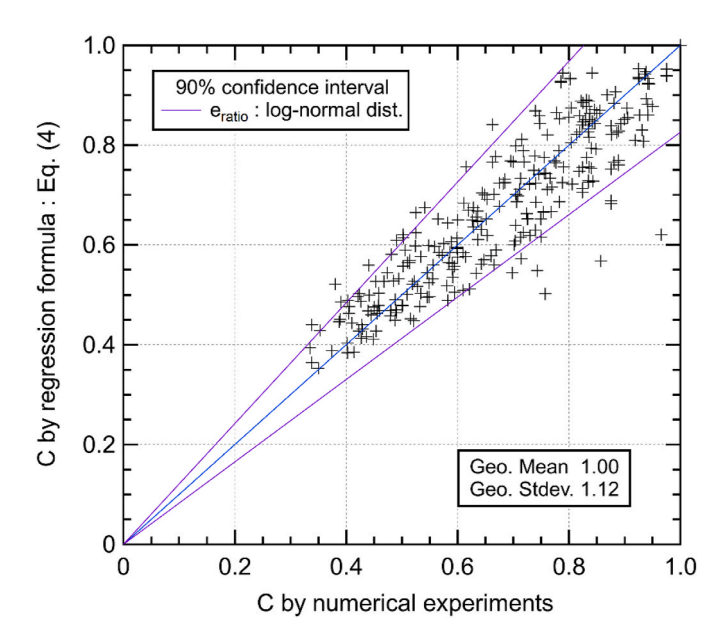


Fig. 12. Comparison of runup reduction factor based on numerical experiments and regression formulas. The blue line reveals the 50% exceedance level. The purple lines reveal the 90% interval under the assumption of log-normal distribution for error ratio.

We note here that the residual-error analysis also indicates that e_{res} follows the normal distribution well with a minimal bias (Bias=0.00) and the RMSE=0.08. Overall, the quantitative agreement is very satisfactory. It is recommended to use the proposed formula within the range of the selected numerical dataset: $0 \le W_B^* < 1.4$, $-0.6 < S^* < 0.9$, and $0.004 < G^* < 0.025$.

Here the present model is briefly compared with the PC16 model. The prediction equations used in the PC16 model were also included in Fig. 10. The PC16 formulas roughly correspond to the middle and lowest values of C of the present model. An additional comparison between the reduction factors in the numerical experiments and the PC16 model indicated substantial scattering. A comparison of the r^2 , RMSE, and bias (Table 2) reveals that the accuracy of the present model is significantly improved compared with the PC16 model.

The comparison with the formulas proposed in EurOtop (2007, 2018) and TAW (2002) is then described briefly. We should note here that the direct quantitative comparison is difficult for the following reasons: The formulas in these manuals are expressed in terms of the wave properties at the toe of the structure, and it is not straightforward to uniquely define the location of the toe in the simple profile used in this study; Besides, the different definition is used for normalized berm width. Accordingly, only the qualitative comparison is mentioned here. On the influence of the relative berm width, the overall tendency of reduction variability is qualitatively similar among the present study, PC16, EurOtop, and TAW, in the sense that the reduction effect becomes stronger with the berm width while it approaches the asymptotic limit for sufficiently wide berms. The comparison on the influence of the relative surge level can be summarized as follows; First, the possible range of reduction (related to K_1) is different among the models. In the present model, the asymptotic values depend on S^* and G^* . The reduction factor could reach 0.4 or less under certain conditions,

Table 2 Comparison of the residual error in \mathcal{C} between PC16 and the present models.

Model	r^2	RMSE	Bias
Proposed Model: Eq. (4)	0.88	0.08	0.00
PC16 Model: Eq. (5e)	0.57	0.17	-0.11
PC16 Model: Eq. (5f)	0.57	0.14	0.04

corresponding to the numerical experiments. On the other hand, the minimum value in the reduction factor in EurOtop and TAW is always limited to 0.6 (irrespective of S^* or G^*). Concerning the dependence of the reduction sensitivity on the relative surge level (related to K_2), the formulations in the present study, TAW, and EurOtop, are generally similar in the sense that the reduction is most intense around S^* =0, and the berm effects decrease as $|S^*|$ increases. The cosine function is used in all these models when S^* >0, while the formulation is different when S^* <0. In the present study, the hyperbolic tangent function is used in terms of the dimensionless surge level to incident wave height, while the variability is expressed by the cosine function in terms of the dimensionless surge level to the maximum runup in EurOtop and TAW.

3.3. Establishment of a conversion formula between the runup based on different definitions

Mase et al. (1983) and Mase and Iwagaki (1985) conducted a series of hydraulic experiments to investigate the influences of wave groupness on the runup of irregular waves. The experiments were conducted for a planar beach with different slopes of 1/5, 1/10, 1/20, and 1/30. In each value of the slope, 30 cases of runup observations were conducted. Based on these hydraulic experiments, Fig. 13 describes the variation of the ratio of the number of runup and incident waves ($n = N_R/N_I$) against the Iribarren number (ξ_p) based on peak period and foreshore slope. The value of n increases with ξ_p and asymptotes to unity. The following regression formula successfully describes the relation between n and ξ_p .

$$n = \tanh \left[\left(0.070 + \frac{\xi_p}{1.5} \right)^{0.80} \right] \tag{14}$$

It is recommended to use Eq. (14) in the range of ξ_p < 3.

Based on the analysis of their hydraulic experiments, Mase et al. (2004) demonstrated that the distribution of runup on the seawall is well described by the Rayleigh distribution. If we assume the Rayleigh distribution for runup, the exceeding probability for a runup value R is expressed as

$$P(R) = \exp \left[-\frac{\pi}{4} \left(\frac{R}{\overline{R}} \right)^2 \right]$$

in which \overline{R} represents mean runup. The ratio of $R_{2\%,I}$ and $R_{2\%,R}$, that is based on the number of incident waves in deep water (N_I) and the number of runup waves (N_R) , respectively, can then be expressed as

$$\frac{R_{2\%,R}}{R_{2\%,I}} = \left[1 + \frac{\ln(n)}{\ln(0.02)}\right]^{1/2} \tag{15}$$

The value of n in Eq. (15) can be determined from Eq. (14). This formula enables us to exchange the $R_{2\%}$ values based on different definitions.

The variation of the conversion coefficient defined by Eq. (15) against ξ_p is shown in Fig. 14. It is compared with the results of the

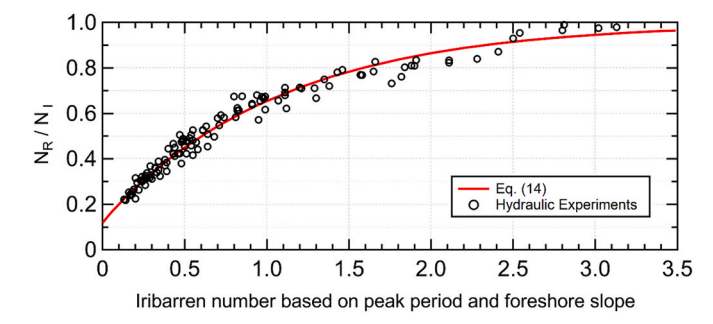


Fig. 13. Variation of the ratio between the number of runup and incident waves against the Iribarren number.

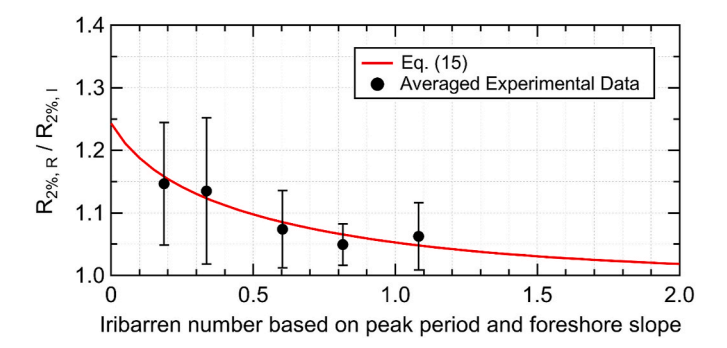


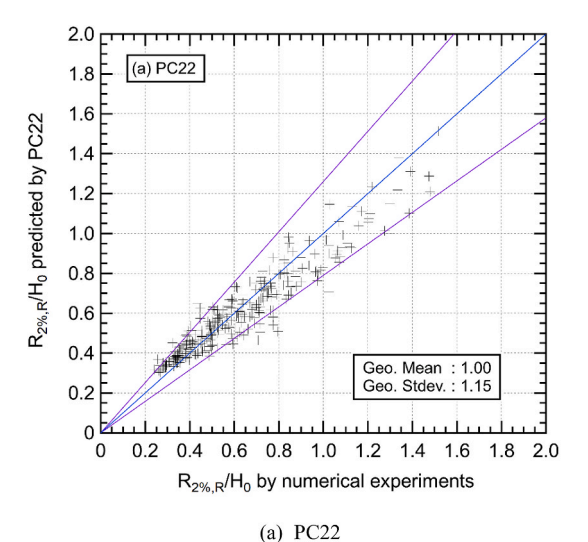
Fig. 14. Variation of conversion coefficient against the Iribarren number.

hydraulic experiments by Mase et al. (2006) and Tamada et al. (2011), which are classified into several classes according to the Iribarren number. The mean and standard deviation in each class are included in the figure. We should note that the scattering of the experimental results in Fig. 14 is not small; The standard deviation observed in the conversion rate is up to around 10%. This implies that the relation between n and ξ_p can be influenced by additional factors. Besides, although the range of ξ_p in the present numerical experiments is within the ranges of Figs. 13 and 14, the foreshore slope used in this study (1/50) is out of the range (1/10 to 1/30) of the experiments by Mase et al. (1983) and Mase and Iwagaki (1985). On the other hand, it can be confirmed that Eq. (15) reproduces the general tendency in the hydraulic experiments well. Overall, we assume that the conversion rate based on Eqs. (14) and (15) are applicable as the first approximation in this study.

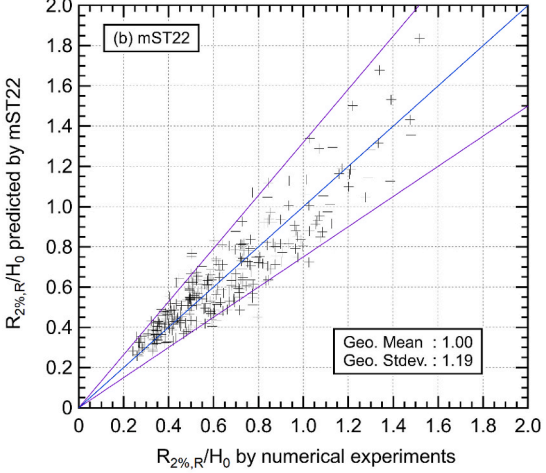
3.4. Performance tests of the proposed model

Finally, the reduction formula represented as Eq. (4) was implemented in PC22 (Eq. (6)), mST22 (Eq. (7)), and IFORM (Eq. (9)), and the applicability of the proposed method was examined against the numerical experiments with wide berms. A consistent comparison was conducted based on $R^*_{2\%,R}$. In IFORM, the following two-step procedure was adopted. First, the dimensionless 2% runup defined with the number of incident waves was computed with the proposed reduction factor. Next, the corresponding 2% runup defined with the number of runup waves was estimated based on Eqs. (14) and (15). In PC22, the coefficient in Eq. (6) was set as a=0.93 empirically to obtain the best fit. Fig. 15 clearly demonstrate that the predictions based on PC22, mST22, and IFORM with the proposed reduction formula can reproduce the characteristics of the runup variabilities in the numerical experiments over a wide range of conditions. The results suggest that the proposed reduction factor is applicable to various kinds of empirical formulas.

In the prediction of the runup, the inclusion of uncertainty is inevitable due to the stochastic nature of runup phenomena and the limitation of model representation. For instance, in the proposed model, prediction error may arise from the combinations of the various formulas used in PC22, mST22, and IFORM, data conversion, and the reduction factor. In order to inspect the characteristics of the error in the model prediction, the distributions of residual error and error ratio were examined. The obtained results indicated that the uncertainty in the runup prediction appeared in different forms depending on the selected empirical model. For the PC22 and mST22 models, the distribution of e_{ratio} followed the log-normal distribution. The geometric mean was 1.00 for both models: Namely, the runup prediction indicated no bias and provided the 50% exceedance level in the numerical experiments (the blue lines in Fig. 15 (a) and (b)). The corresponding geometric standard deviations were 1.15 and 1.19 for PC22 and mST22 models, respectively. Under the assumption of log-normal distribution for e_{ratio} , the PC22 and mST22 models predicted 90% of the normalized runup on a dune within a range of relative error of less than approximately 20–25% and 25-30%, respectively. The 90% intervals for these two models are



(-)



(c) IFORM

Fig. 15. Comparison of normalized runup based on numerical experiments and prediction models. The blue lines reveal the 50% exceedance level. The purple lines in (a) and (b) reveal the 90% confidence interval under the assumption of log-normal distribution for error ratio. The green lines in (c) indicate the 90% confidence interval under the assumption of normal distribution for residual error.

indicated by purple lines in Fig. 15 (a) and (b). On the other hand, the prediction uncertainty in IFORM was found to follow a normal distribution of the residual error (e_{res}). The predictions by IFORM indicated a high correlation (r^2 =0.88) and a small positive bias (Bias=0.05). The 50% exceedance level is indicated by the blue line in Fig. 15 (c): IFORM provided slightly conservative estimates when the normalized runup was relatively small. The corresponding RMSE was 0.13. Under the assumption of normal distribution for e_{res} , 90% of the plots were located within the green lines (approximately within prediction \pm 0.2) in Fig. 15 (c).

In summary, the quantitative agreement was quite satisfactory for all three models. The direct quantitative comparison with EurOtop was not conducted because of the same reasons that were mentioned in the last part of Section 3.2.

3.5. Limitation of the proposed model and possibilities of further applications

In this section, we briefly address some of the limitations of the proposed model and suggest some future needs of research for improvement and possibilities for further applications.

First, in this study, the proposed formula for the reduction factor is developed against the numerical experiments under idealized conditions of a dune-berm-foreshore system. Although a fairly wide range of conditions is covered in the numerical experiments by referring to the field observations, there still remain certain limitations. On the morphological aspects, the slopes of the foreshore, dune, and berm were fixed in the numerical experiments. For surge level, Figs. 6(a) and 8(a) indicate that available data seems insufficient in the range $0.3 < S^* < 0.8$. Besides, some of the physical phenomena are not taken into account in the model. For example, no morphological change during large storm events was considered. The influence of surface roughness (vegetation) and percolation also needs additional studies. The oblique incidence of incoming waves, the effects of alongshore variability in bathymetry and topography, and the influence of the three-dimensional evolution of infragravity waves along the coastlines should also be considered in the future. The combined use of additional influence factors describing the above phenomena deserves further investigation.

Second, the inherently stochastic nature of wave runup inevitably produces aleatory uncertainty. Hedges and Reis (1998) assumed a Rayleigh distribution to the runup and expressed the p % confidence value (a level below which p % of the cases should lie) of the maximum runup (R_{max}) as follows:

$$(R_{max})_{p\%} = \left[\frac{1}{2} \left(\ln N_R - \ln \left(-\ln \frac{p}{100} \right) \right) \right]^{1/2} R_{1/3}$$
 (16)

where $R_{1/3}$ is the significant wave runup defined as the average of the highest one-third of the runup and N_R is the number of runup events. In the equation above, p=37 provides the most probable value in observations. If we consider the most probable value, Eq. (16) reveals that a relative difference of approximately 10 (20) % may arise between $R_{\rm max}/R_{1/3}$ for $N_R=250$ (100) and 1000.

Recent studies examined the uncertainties in the numerical evaluation of runup (McCabe et al., 2013; Torres-Freyermuth et al., 2019; Rutten et al., 2021) and overtopping (e.g., Palemón-Arcos et al., 2015; Romano et al., 2015) originating from the random assignment of starting phases into the harmonic components of the irregular-wave sequences at the incident boundary. These studies revealed that the strength of the aleatory uncertainty depends on the length of the wave time series used in the numerical simulations. The numerical experiments for wave runup by McCabe et al. (2013), Rutten et al. (2021), and Torres-Freyermuth et al. (2019) demonstrated that the relative uncertainty originating from wave randomness is up to approximately 15% when N_I is around 100. If we collate the wave number used in the present numerical experiment (N_I =250) and these statistical and numerical

considerations, it is reasonable to assume that each run in the numerical experiments in the present study includes a random relative error of around 10%. However, this is well within the typical strength of scattering of the plots obtained by hydraulic experiments against the empirical regression formula for runup (e.g., Fig. 10 in Mase et al. (2013)).

In order to cope with the problem arising from wave randomness, Reis et al., (2008) suggested the use of multiple short sequences of waves. The use of ensemble simulation of 15 ~ 30 runs is suggested in Romano et al. (2015), Rutten et al. (2021), Palemón-Arcos et al. (2015), Torres-Freyermuth et al. (2019) when N_I is around 100. In Figs. 6 and 8, several data points are included for the same (or closely adjacent) values of the governing parameters (W_B^* , S^* , and G^*). Similar to the ensemble simulations, the random errors in these plots are considered to be averaged out to some extent in the course of regression analysis. Taking into account that the run-time of each simulation (2500 ~ 5000 s) is comparable to the typical record length in the field (900 ~ 10800 s) (Rutten et al., 2021; Stockdon et al., 2006), the use of the combination of several runs over such duration is reasonable. Furthermore, we should note that the empirical prediction models should be used for the preliminary design. The required level in prediction accuracy is quantitatively different from the elaborated numerical computations or hydraulic scale model tests for a specific case in the final stage. Overall, we assume that the aleatory uncertainty around 10% is acceptable for the development of the general form of the reduction factor used in empirical runup prediction models.

Third, the applicability of the prediction formula has been 'validated' against the same dataset for the model construction in this study. Although the range of conditions in the numerical experiments is determined referring to the field observation, the comparison of the results with raw data of the runup reduction in the actual field is missing. Further comparison with independent data sources, especially from the field and large-scale laboratory observations, is desirable in order to complete the full validation of the model.

Since the proposed model includes the relative water level and offshore wave properties as the governing parameters, it can be applied to make quick and robust estimates of the influence of temporally varying surge levels and wave properties over relatively short (storm events) or a long (climate change) time scale. Similarly, it may be interesting to apply the present model to examine the variability of the dissipation effects of coral reefs on runup and overtopping (e.g., Kawasaki et al., 2008; Liu et al., 2020) under the expected future sea-level rise. Concerning the influence of the morphological change of the profile, the proposed model could be used to roughly estimate the variability of runup reduction due to the berm at the early stage of a large storm. With the progress of the storm, the berm width is expected to decrease. The proposed relationship is able to identify, for a given normalized surge level and wave properties, the minimum berm width below which the beneficial effects of the berm start to decrease. Moreover, the proposed model can be used together with other (empirical) models that are able to estimate, at least roughly, the decrease of berm width during storms as an example of a more advanced application.

4. Summary remarks

This study formulates the reduction effects of a sandy berm on irregular wave runup over a dune-berm coast. Based on the reexamination of the numerical experiments by PC2016, the relationships among the dimensionless runup on a dune, berm width, relative surge level, and wave steepness in deep water were investigated in detail. An empirical reduction formula has been developed through a sequence of regression analyses, and its validity was examined against the numerical experiments. In addition, conversion formulas between representative runup values based on different statistical definitions have been derived. The proposed reduction formula was then implemented into empirical runup models, and the applicability of the

proposed method was validated through consistent comparisons based on the statistical conversion formulas for normalized runup. The main results obtained in this study can be summarized as follows.

A dimensionless factor (C) describing the reduction effects on runup due to a wide berm was formulated empirically as a function of normalized berm width, relative surge level, and wave steepness (Eqs. (4) and (10) \sim (13), Fig. 10). The developed formula for the reduction effects compared very well with the numerical experiments over a broad range with no bias and a 90% confidence interval of approximately 20% relative error (Figs. 11 and 12). The proposed formula is applicable within the range $0 \leq W_B^* < 1.4$, $-0.6 < S^* < 0.9$, and $0.004 < G^* < 0.025$.

The conversion formulas between representative runup values based on different statistical definitions have been developed based on hydraulic experiments and an assumption of Rayleigh distribution of runup (Eqs. (1), (14) and (15)). The validity of the conversion formulas was confirmed through comparison with a hydraulic experiment. The derived formulas enabled the consistent comparisons among $R_{2\%,I}$, $R_{2\%,R}$, and $R_{1/50,R}$.

The proposed reduction formula was then implemented into three empirical runup models: PC22 (Eq. (6)), mST22 (Eq. (7)), and IFORM (Eq. (9)). The comparison with numerical experiments demonstrated that all three models with the proposed reduction formula satisfactorily reproduced $R_{2\%,R}^*$ over a broad range in the numerical experiments (Fig. 15). On the other hand, the appearance of prediction uncertainty depended on the model selection. The error ratio in PC22 and mST22 followed a log-normal distribution. The corresponding 90% confidence interval was within approximately $20 \sim 30\%$ of relative error (Fig. 15a and b). When the formula was combined with IFORM, the residual error followed a normal distribution. The model prediction indicated a small conservative bias (+0.05) and RMSE of 0.13 for $R_{2\%,R}^*$ (Fig. 15(c)).

The reduction factor and the conversion formula have been derived based on numerical and hydraulic experiments, respectively. These formulas were constructed independently of the runup models used in this study. In addition, the implementation is straightforward because it needs only to multiply the reduction factor or conversion coefficient to the prediction of existing runup models. The satisfactory agreement in Fig. 15 for all the three models revealed that the implementation of the

reduction factor and the conversion formula into other prediction models for runup is expected to be effective.

The proposed formulas of runup reduction were derived based on a synthetic dataset over a fairly wide range of conditions. However, there remain several limitations in model developments and validations. Incorporating additional physical aspects and full validation with independent data sources from the field and large-scale laboratory observations are highly desirable to further improve the model in the future.

CRediT authorship contribution statement

Masatoshi Yuhi: Conceptualization, Methodology, Investigation, Formal analysis, Visualization, Writing - original draft, Funding acquisition. Hajime Mase: Conceptualization, Supervision, Writing - review & editing, Funding acquisition. Daniel T. Cox: Investigation, Writing - review & editing. Hyoungsu Park: Investigation, Writing - review & editing.

Declaration of competing interest

The authors declare that they have no known competing financial interests or personal relationships that could have appeared to influence the work reported in this paper.

Acknowledgments

This work is partially supported by the Grants-in-Aid for Scientific Research by the Japan Society for the Promotion of Science [Grant No. 19H02403, 20H02256] and the collaborative research program of the Disaster Prevention Research Institute of Kyoto University [Grant No. 30G-09]. Suggestive comments from Prof. Hiraishi (Kyoto Univ.), Prof. Umeda (Kanazawa Univ.), Dr. Kim (Kumamoto Univ.), Dr. Kawasaki, and Dr. Mizutani (Hydro Technology Institute Co., Ltd.) are appreciated. Assistance rendered by Mr. Ohtani (a former student of Kanazawa Univ.) and Ms. Ichimura (a former graduate student of Kanazawa Univ.) is acknowledged. Constructive comments and suggestions from the anonymous reviewers are highly appreciated.

Nomenclature

C reduction factor of runup on a dune

 C_{PC} reduction factor used in Park and Cox (2016).

 e_{ratio} error ratio between model prediction and numerical experiment e_{res} residual error between model prediction and numerical experiment

 G^* wave slope in deep water

 H_0 deep-water significant wave height

 h_B berm height with respect to still water line

 h_{br} breaker depth

 h_D dune height with respect to berm level

 K_1 a parameter describing the maximum reduction effect K_2 a sensitivity parameter controlling runup reduction

 L_0 wavelength in deep water N_R number of runup events

 N_I number of incident waves in deep water

n the ratio between the number of runup and incident waves

 r^2 coefficient of determination $R_{1/50}$ average of highest 2% runup

 $R_{1/50, R}$ $R_{1/50}$ based on the number of runup waves

 $R_{2\%}$ runup exceeded by 2% of waves

 $R_{2\%}^*$ normalized 2% runup

 $R_{2\%,I}$ $R_{2\%}$ based on the number of incident waves in deep water

 $R_{2\%,R}$ $R_{2\%}$ based on the number of runup waves

- S surge level
- S* normalized surge level
- T_p peak period W_B berm width
- W_B^* normalized berm width W_D dune width on berm level
- eta_d dune slope eta_f foreshore slope eta_{im} imaginary slope
- β_{im} imaginary slope β_t transition slope
- ξ_d Iribarren number based on dune slope ξ_f Iribarren number based on foreshore slope ξ_{im} Iribarren number based on imaginary slope ξ_r Iribarren number based on representative slope

References

- Almar, R., Ranasinghe, R., Bergsma, E.W.J., Diaz, H., Melet, A., Papa, F., Vousdoukas, M., Athanasiou, P., Dada, O., Almeida, L.P., Kestenare, E., 2021. A global analysis of extreme coastal water levels with implications for potential coastal overtopping. Nat. Commun. 12, 3775. https://doi.org/10.1038/s41467-021-24008-9
- Battjes, J.A., 1974. Surf similarity. In: Proc. 14th Int. Conference on Coastal Eng. Conf., pp. 466–480.
- Burcharth, H.F., Andersen, T.L., Lara, J.L., 2014. Upgrade of coastal defense structures against increased loadings caused by climate change: a first methodological approach. Coast. Eng. 87, 112–121 (coasts@Risks: THESEUS, a new wave in coastal protection. URL. http://www.sciencedirect.com/science/article/pii/S037838 331300212.
- Coastal Development Institute of Technology (CDIT), 2018. The Technical Standards and Commentaries for Coastal Facilities in Japan, revised edition. The Ports and Harbours Association of Japan, p. 347 (in Japanese).
- EurOtop, 2007. In: Pullen, T., Allsop, N.W.H., Kortenhaus, A., Schüttrumpf, H., Van der Meer, J.W. (Eds.), Wave Overtopping of Sea Defenses and Related Structures: Assessment Manual, p. 178. www.overtopping-manual.com.
- EurOtop, 2018. In: Van der Meer, J.W., Allsop, N.W.H., Bruce, T., De Rouck, J., Kortenhaus, A., Pullen, T., Schüttrumpf, H., Troch, P., Zanuttigh, B. (Eds.), Manual on Wave Overtopping of Sea Defenses and Related Structures. An Overtopping Manual Largely Based on European Research, but for Worldwide Application, p. 320. www.overtopping-manual.com.
- Guza, R.T., Thornton, E.B., 1982. Swash oscillations on a natural beach. J. Geophys. Res. Oceans 87 (C1), 483-491.
- Hedges, T.S., Reis, M.T., 1998. Accounting for random wave run-up in overtopping predictions. Proc. Inst. Civil Eng., Maritime Eng. 157, 113–122.
- Holman, R.A., 1986. Extreme value statistics for wave run-up on a natural beach. Coast. Eng. 9 (6), 527–544.
- Kawasaki, L., Kiku, M., Sasada, Y., 2008. Numerical and experimental study on wave deformation and overtopping around vertical seawall in coral reef sea area. Proc. 18th Int. Offshore and Polar Eng. Conf. 698–705.
- Kraus, N.C., Rosati, J.D., 1997. Interpretation of Shoreline-Position Data for Coastal Engineering Analysis (No. CERC-CETN-II-39) Coastal Engineering Research Center. Vicksburg Ms.
- Liu, Y., Lib, S., Chena, S., Huc, C., Fand, Z., Jina, R., 2020. Random wave overtopping of vertical seawalls on coral reefs. Appl. Ocean Res. 100, 102166.
- Lynett, P., Liu, P.L.F., 2005. A numerical study of the run-up generated by three-dimensional landslides. J. Geophys. Res. Oceans 110 (C3). https://doi.org/10.1029/2004JC002443.
- Lynett, P., Borrero, J., Liu, P.L.-F., Synolakis, C.E., 2003. Field survey and numerical simulations: a review of the 1998 Papua New Guinea tsunami. Pure Appl. Geophys. 160, 2119–2146.
- Lynett, P., Melby, J., Kim, D.-H., 2010. An application of Boussinesq modeling to hurricane wave overtopping and inundation. Ocean Eng. 37, 135–153.
- Lynett, P.J., Wu, T.-R., Liu, P.L.-F., 2002. Modeling wave runup with depth-integrated equations. Coast Eng. 46 (2), 89–107.
- McCabe, M.V., Stansby, P.K., Apsley, D.D., 2013. Random wave runup and overtopping a steep sea wall: shallow-water and Boussinesq modeling with generalized breaking and wall impact algorithms validated against laboratory and field measurements. Coast Eng. 74, 33–49.
- Mase, H., 1995. Frequency down-shift of swash oscillations compared to incident waves. J. Hydraul. Res. 33 (3), 397–411.
- Mase, H., Doi, H., Iwagaki, Y., 1983. Experimental study on the influences of wave grouping on the runup of irregular waves. Proc. Coast. Eng., JSCE 19, 114–118 (in Japanese).
- Mase, H., Iwagaki, Y., 1985. Run-up of Random Waves on Gentle Slopes. Proc. 19th Int. Conf. on Coastal Eng., Houston, ASCE, pp. 593–609.
- Mase, H., Kirby, J.T., 1993. Hybrid frequency-domain KdV equation for random wave transformation. In: Proc. 23rd Int. Conf. On Coastal Eng., ASCE, pp. 474–487.

- Mase, H., Miyahira, A., Hedges, T.S., 2004. Random wave run-up on seawalls near shorelines with and without artificial reefs. Coast Eng. J. 46 (3), 247–268.
- Mase, H., Tamada, T., Yasuda, T., Hedges, T., Reis, M., 2013. Wave runup and overtopping at seawalls built on land and in very shallow water. J. Waterway Port Coast. Ocean Eng. ASCE 139 (5), 346–357.
- Mase, H., Tamada, T., Yasuda, T., Kawasaki, K., 2016. Integrated formula of wave overtopping and runup modeling for seawalls. J. JSCE, Ser. B2 (Coastal Eng.) 72 (1), 83–88 (in Japanese).
- Mase, H., Tokoro, Y., Memita, T., Sakurai, H., Imabayashi, T., 2006. Estimation formula for random wave runup on seawalls near shoreline. J. JSCE, Ser. B, 62 (1), 163–168 (in Japanese).
- Nakamura, M., Sasaki, Y., Yamada, J., 1972. Runup on seawalls with composite cross-section. In: Proc. Of Coast. Eng., JSCE, vol. 19, pp. 309–312 (in Japanese).
- Palemón-Arcos, L., Torres-Freyermuth, A., Pedrozo-Acuña, A., Salles, P., 2015. On the role of uncertainty for the study of wave-structure interaction. Coast Eng. 106, 32–41.
- Park, H., Cox, D.T., 2016. Empirical wave run-up formula for wave, storm surge and berm width. Coast Eng. 115, 67–78.
- Park, H., Cox, D.T., Lynett, P.J., Wiebe, D.M., Shin, S., 2013. Tsunami inundation modeling in constructed environments: a physical and numerical comparison of free-surface elevation, velocity, and momentum flux. Coast. Eng. 79, 9–21.
- Raubenheimer, B., Guza, R.T., 1996. Observations and predictions of run-up. J. Geophys. Res. Oceans 101 (C11), 25575–25587.
- Reis, M.T., Neves, M.G., Hedges, T., 2008. Investigating the lengths of scale model tests to determine mean wave overtopping discharges. Coast Eng. J. 50 (4), 441–462. https://doi.org/10.1142/S057856340800182X.
- Romańczyk, W., Boczar-Karakiewicz, B., Bona, J.L., 2005. Extended equilibrium beach profiles. Coast Eng. 52 (9), 727–744.
- Romano, A., Bellotti, G., Briganti, R., Franco, L., 2015. Uncertainties in the physical modeling of the wave overtopping over a rubble mound breakwater: the role of the seeding number and of the test duration. Coast Eng. 103, 15–21.
- Ruggiero, P., Komar, P.D., McDougal, W.G., Marra, J.J., Beach, R.A., 2001. Wave run-up, extreme water levels and the erosion of properties backing beaches. J. Coast Res. 407–419.
- Rutten, J., Torres-Freyermuth, A., Puleo, J.A., 2021. Uncertainty in runup predictions on natural beaches using XBeach nonhydrostatic. Coast Eng. 166, 103869.
- Saville Jr., T., 1958. Wave run-up on composite slopes. In: Proc. 6th Int. Conf. On Coastal Eng. ASCE, Reston, VA, pp. 691–699.
- Sekimoto, T., Isobe, M., Anno, K., Nakajima, S., 2013. A new criterion and probabilistic approach to the performance assessment of coastal facilities in relation to their adaptation to global climate change. Ocean Eng. 71, 113–121.
- Senechal, N., Coco, G., Bryan, K.R., Holman, R.A., 2011. Wave run-up during extreme storm conditions. J. Geophys. Res. Oceans 116 (C7).
- Stockdon, H.F., Holman, R.A., Howd, P.A., Sallenger, A.H., 2006. Empirical parameterization of setup, swash, and run-up. Coast Eng. 53 (7), 573–588.
- Tamada, T., Mase, H., Yasuda, T., 2011. Runup formulation for seawalls near shoreline. In: Proc. Coastal Struct. ASCE. CD-ROM B5-053.
- Tamada, T., Mase, H., Yasuda, T., 2015. Wave runup and overtopping integrated model for vertical seawall based on CLASH datasets. Proc. Scacr2015, Int. Short Course/ Conf. Appl. Coast. Res. 361–370.
- Technical Advisory Committee on Flood Defense (TAW), 2002. In: Van der Meer, J.W. (Ed.), Technical Report Wave Run-Up and Wave Overtopping at Dikes, p. 50. The
- Torres-Freyermuth, A., Pintado-Patiño, J.C., Pedrozo-Acuña, A., Puleo, J.A., Baldock, T. E., 2019. Runup uncertainty on planar beaches. Ocean Dynam. 69, 1359–1371.
- U.S. Army Corps of Engineers (USACE), 2002. Coastal Eng. Manual (CEM). EM 1110-2-1100, Washington, D.C. (in 6 volumes).
- Vitousek, S., Patrick, L., Barnard, P.L., Fletcher, C.H., Frazer, N., Erikson, L., Storlazzi, C. D., 2017. Doubling of coastal flooding frequency within decades due to sea-level rise. Sci. Rep. 7, 1399.
- Yuhi, M., Mase, H., Kim, S., Umeda, S., Altomare, C., 2021. Refinement of integrated formula of wave overtopping and runup modeling. Ocean Eng. 220 (#108350), 15. https://doi.org/10.1016/j.oceaneng.2020.108350.